Atmospheric Environment 309 (2023) 119931

Contents lists available at ScienceDirect

Atmospheric Environment

journal homepage: www.elsevier.com/locate/atmosenv

Changes in first- and second-order sensitivities of ozone concentration to its precursors over the Yangtze River Delta region of China due to COVID-19 lockdown: Insights from CMAQ-HDDM modeling study

Elly Arukulem Yaluk [a,b], Yangjun Wang [a,b,*], Sen Jiang [a,b], Ling Huang [a,b], Guibin Lu [c], Ansheng Zhu [a,b], Jinting Bian [a,b], Jin Xue [a,b], Yufei Du [a,b], Nan Chen [a,b], Kasemsan Manomaiphiboon [d,e], Hui Chen [a,b], Kun Zhang [a,b], Li Li [a,b,**]

[a] School of Environmental and Chemical Engineering, Shanghai University, Shanghai, 200444, China
[b] Key Laboratory of Organic Compound Pollution Control Engineering (MOE), Shanghai University, Shanghai 200444, China
[c] School of Economics, Shanghai University, Shanghai, 200444, China
[d] The Joint Graduate School of Energy and Environment, King Mongkut's University of Technology, Thonburi, Bangkok 10140, Thailand
[e] Center of Excellence on Energy Technology and Environment, Ministry of Higher Education, Science, Research and Innovation, Bangkok, 10140, Thailand

HIGHLIGHTS

- Negative contribution of chemistry to O_3 was significantly weakened due to COVID-19 lockdown.
- 1^{st}- and 2^{nd}-order O_3 sensitivities to NO_x were negative and positive, respectively.
- 2^{nd}-order O_3-NO_x sensitivity increased 3 times due to COVID-19 lockdown.
- Higher rate of O_3 increase due to NO_x reductions during COVID-19 lockdown.

ARTICLE INFO

Keywords:
Ozone
CMAQ
HDDM-3D
Sensitivity analysis
COVID-19
Yangtze River Delta

ABSTRACT

Elevated ozone (O_3) concentration during the COVID-19 lockdown is a matter of great concern, but the changes of its sensitivities to key precursors remains unclear. This study utilized the Community Multiscale Air Quality (CMAQ) model coupled with the Higher-order Decoupled Direct Method in Three Dimensions (HDDM-3D) and the process analysis (PA) modules to reveal in detail the changes in O_3-precursors sensitivities and the contribution of major chemical and physical processes to O_3 formation/loss during the month-long COVID-19 lockdown in early 2020 over the Yangtze River Delta (YRD) region of China. The results indicate that the contributions (absolute value) of gas-phase chemistry to O_3 and O_x (i.e., O_3+NO_2) were reduced by 35–50% and 8–24%, respectively, under lockdown-specific (LCD) scenario compared with the business-as-usual (BAU) scenario in the highly urbanized areas of eastern and central YRD. Under the BAU (LCD) scenario, the first-order and second-order O_3-NO_x sensitivities averaged about −25 (−36) μg/m^3 and about 8 (28) μg/m^3, respectively. These 1^{st}- and 2^{nd}-order sensitivities of O_3 to NO_x were both intensified due to COVID-19 lockdown, which potentially contributed to O_3 increases of between 5 and 10 μg/m^3. In other words, the concentration of O_3 and its rate of increase were both amplified due to COVID-19 lockdown. Overall, this study highlighted a significant wintertime "NO_x reduction disbenefit" phenomenon over YRD because of both strong 1^{st}-order (negative) and 2^{nd}-order (positive) O_3 sensitivities to NO_x emissions, which were further reinforced due to COVID-19 lockdown.

* Corresponding author. School of Environmental and Chemical Engineering, Shanghai University, Shanghai, 200444, China.
** Corresponding author. School of Environmental and Chemical Engineering, Shanghai University, Shanghai, 200444, China.
E-mail addresses: yjwang326@shu.edu.cn (Y. Wang), lily@shu.edu.cn (L. Li).

https://doi.org/10.1016/j.atmosenv.2023.119931
Received 26 January 2023; Received in revised form 20 June 2023; Accepted 26 June 2023
Available online 6 July 2023

1. Introduction

The emergence of the COVID-19 outbreaks since late 2019 created an extreme global disruption of human life. In response, the government of the People's Republic of China (PRC) quickly activated national emergency containment protocols to reduce the intensity of the epidemic, which included stringent "stay-at-home" policy known as the "COVID-19 lockdown" (Tian et al., 2020). This necessitated the closure, halting or lessening of industrial operations, transportation services, construction works, restaurant and catering facilities, educational institutions, among others. This massive embargo led to substantial reduction of major air pollutant emissions (Muhammad et al., 2020) and an overall improvement of air quality in China (Liu et al., 2021; Pei et al., 2020). However, during the same period several Chinese cities experienced significant increases in the concentrations of ground-level ozone (O_3) (Lian et al., 2020; Pei et al., 2020; Wang et al., 2020b; Zhao et al., 2020). This peculiar O_3 increases during the lockdown period were also reported in some cities in Europe (Collivignarelli et al., 2020; Ordóñez et al., 2020; Sicard et al., 2020), South America (Cazorla et al., 2021; Siciliano et al., 2020), as well as in India (Shehzad et al., 2020).

Understandably, O_3 formation is usually a nonlinear chemical process strongly dependent on the concentrations of nitrogen oxides ($NO_x = NO_2+NO$), volatile organic compounds (VOCs) as well as the intensity of sunlight (Atkinson, 2000). Once these precursors are emitted into the troposphere, instant O_3 formation is initiated via a rapid and coupled sequence of radical cycles involving NO_x and RO_x (i.e., organic peroxy (RO_2), hydroperoxy (HO_2) and hydroxyl (OH)) (Li et al., 2018; Wang et al., 2017). This mechanism, although more complex in real atmosphere, forms the core of the photochemical formation of tropospheric O_3. In principle, any changes that can influence the sources of NO_x and VOCs emissions would significantly impact the O_3-precursors relationship and ultimately result in an unexpected O_3 formation outcome (Tang et al., 2021), which was evident during the COVID-19 lockdown period (Liu et al., 2021). Therefore, it is prudent to gain deeper insights into the underlying response of O_3 following the drastic reductions of NO_x and VOC emission during the lockdown period. This will significantly benefit ongoing and prospective O_3 control strategies.

Over the Yangtze River Delta (YRD) region which is one of the world's largest urban agglomerations in the world, a number of recent studies have made significant attempts to understand the dramatic increase in O_3 levels during COVID-19 lockdown. Wang et al. (2021) linked these O_3 increases to an enhancement of the atmospheric oxidation capacity (AOC), similar to the findings by Zhu et al. (2021). In sharp contrast, another study by Wang et al. (2022a) reported a widespread reduction of AOC over the YRD region during the same lockdown period, and noted a significant decline in the chemical consumption of O_3 by nitric oxide (NO) to have had an overwhelming effect that resulted in net O_3 increase. In addition, some studies reported a dramatic shift in O_3-precursors sensitivity regimes over YRD during the lockdown period. For instance, using photochemical indicator ratios (PIRs) Zhu et al. (2021) and Wang et al. (2021) applied the ratios of formaldehyde (HCHO) to NO_2 columns, and hydrogen peroxide (H_2O_2) to nitric acid (HNO_3) production rates, respectively, and found a conspicuous change of O_3 chemical regimes from VOC-limited regimes to NO_x-limited during the lockdown period. On the other hand, using an observation-based model (OBM) Zhang et al. (2022) also noted that O_3 formation conditions switched from VOC-limited to the border of a NO_x- and VOC-limited regime. However, it should be noted that PIRs are entirely based on O_3 formation (and not O_3 removal) and therefore do not account for photochemical aging.

Actually, accurate diagnosis of these regimes (especially for NO_x-titration) is usually quite challenging (Sillman and West, 2009). NO_x--titration is typically dominant in areas (and time) with intense sources of directly emitted NO_x, and therefore O_3 concentrations are consumed by the reaction $O_3+NO \rightarrow NO_2$ rather than photochemical production (Sillman and He, 2002). For OBMs, since it does not consider the effect of atmospheric transport, which has a great influence on the concentration change of ozone at a given location, this method is also insufficient in diagnosing the sensitivity of ozone to precursors. Moreover, the application of OBMs is very limited in space because it is based on observational data.

Three-dimensional chemical transport models (CTMs) have unique advantages in studying the sensitivity of ozone to precursors because they include emissions, chemical processes, atmospheric transport, and deposition. Over the past decade, state-of-the-art CTMs have been sufficiently equipped with tools that can adequately characterize complex atmospheric relationships such as that of O_3 and its precursors (Liu et al., 2020; Sharma et al., 2017). For instance, the Community Multiscale Air Quality (CMAQ) model (Byun and Schere, 2006) in the recent past was instrumented with a powerful higher-order sensitivity analysis tool (i.e., the HDDM-3D, Higher-order Decoupled Direct Method in Three Dimensions) (Hakami et al., 2003), which can efficiently and simultaneously compute O_3-NO_x-VOCs sensitivities (Cohan et al., 2005) while accounting for nonlinear interactions (Arter and Arunachalam, 2021). Moreover, sensitivity outputs from HDDM-3D have been utilized to identify the sources contributing to O_3 formation over east Asia (Itahashi et al., 2015); for innovative construction of O_3 isopleths to support abatement strategies in China (Shen et al., 2021a); as well as to investigate O_3-NO_x-VOCs sensitivities and characterize O_3 chemical regimes during a severe pollution episode in YRD (Wang et al., 2022b). Although the traditional CTM-based brute force method (BFM) can achieve relatively similar results, the HDDM method has been found to be more flexible and efficient in implementation particularly for several sensitivity parameters notwithstanding the computing resources required (Huang et al., 2017; Shen et al., 2021b; Zhang et al., 2012). Moreover, HDDM-3D not only can quantitatively identify the sensitivity of O_3 to precursor emissions, but also can quantify the response of this sensitivity to changes in precursor emissions based on the second-order sensitivity coefficients, which are of great importance for ozone pollution mitigation decision-making.

In this work, the CMAQ-HDDM-3D method was adopted to comprehensively reveal the changes of the first- and second-order sensitivities of O_3 to its precursors in the YRD region during the COVID-19 lockdown. This way, we can explore in detail the responsiveness of O_3 to the substantial changes in anthropogenic emissions of its precursors, and eventually uncover important insights into the underlying cause of elevated O_3 levels observed during the lockdown period. Although the overall COVID-19 lockdown policy was effected from 24th January to 31st March over the YRD region, this study focused on the period from 24th January to around February 24th, 2020 (i.e., when strict "Level-I" measures were effected, hereafter referred to as LD-I) (Li et al., 2020). In addition, we also utilized the process analysis (PA) tool embedded in CMAQ to examine the changes in contributions of physical and chemical processes to ozone during COVID-19 lock down period.

2. Methodology

2.1. Model configuration

A set of three integrated modelling systems consisting of a CTM, regional meteorological model and an emission processor, were configured to adequately cover both the pre-lockdown (PLD) and LD-I study period between 6th January to February 24, 2020. As shown in Fig. 1, Lambert Conformal map projection and three domains with horizontal resolutions of 36 km, 12 km, and 4 km, respectively, were used in this study. These domains were vertically divided into 14 layers. The innermost/target domain covers the entire YRD region, which includes the three provinces of Zhejiang, Jiangsu and Anhui and the municipality of Shanghai. There are 41 prefecture cities in the YRD region and Hangzhou, Nanjing, and Hefei are the capital cities of Zhejiang, Jiangsu, and Anhui provinces, respectively. In this study, we focus on at least one typical urban site in Shanghai (Jing'an: JA), Hangzhou

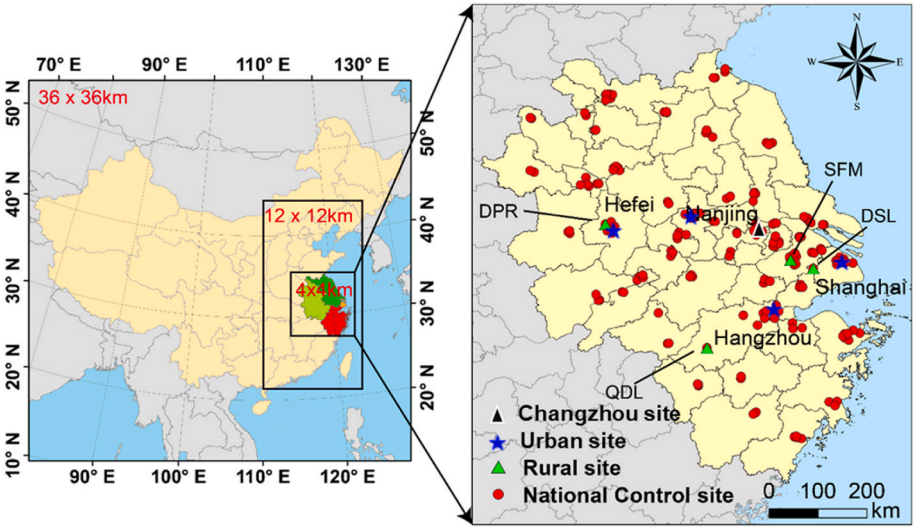

Fig. 1. Modeling domains and locations of the national observational sites. The four rural sites are Dianshan Lake (DSL), Qiandao Lake (QDL), Dongpu Reservoir (DPR) and Shangfang Mountain (SFM).

(Wolong bridge: WB), Nanjing (Caochangmen: CM) and Hefei (Mingzhu square: MS), as well as four other typical rural/suburban sites of YRD region that includes Dianshan Lake (DSL), Qiandao Lake (QDL), Dongpu Reservoir (DPR) and Shangfang Mountain (SFM) (Fig. 1).

The CMAQ model version 5.3.3 was used to simulate air quality. PA and HDDM-3D tools embedded in the CMAQ model provided the outputs to analyse processes and O_3-NO_x-VOCs sensitivities, respectively. The Weather Research and Forecasting (WRF) model version 4.0 (Skamarock et al., 2019) was used to generate the meteorological inputs required to drive the CMAQ model. Additionally, the Sparse Matrix Operator Kernel Emissions model (SMOKE, https://www.cmascenter.org/smoke) was used to process the anthropogenic emissions files into a format suitable for the CMAQ model. The air quality simulation for the areas outside YRD were based on the multi-resolution (anthropogenic) emission inventory for China (MEIC, http://www.meicmodel.org/). The emission inventory of the YRD region used in this work is the same as what was utilized in a previous study (Li et al., 2020). The Model of Emissions of Gases and Aerosols from Nature (MEGAN) (Guenther et al., 2012) version 3.0 (http://bai.ess.uci.edu/megan) was used to generate the biogenic emission inventory. The domain setup and configurations used in this work are the same that were utilized in a recent study (Wang et al., 2022b).

2.2. Simulation scenarios

In this study, CMAQ model was configured to simulate two distinct scenarios. The first simulation scenario (hereafter referred to as the BAU scenario) was run with "normal" or "business-as-usual" anthropogenic emissions during the COVID-19 lockdown period (from 24th January to around February 24th, 2020, the LD-I period mentioned above). The other simulation scenario (hereafter referred to as the LCD scenario) was run with an anthropogenic emissions inventory after changes in emissions caused by the lockdown during the COVID-19 lockdown period (LD-I period mentioned above). It is also noteworthy that there were great changes of the emissions of a number of pollutants during the LD-I lockdown period compared with the normal scenario (BAU). These various changes of emissions associated with the changes of the activity data in various sectors during the lockdown period (LCD scenario) was estimated by Li et al. (2020), as shown in Table S1, which reflects the perturbations of anthropogenic emissions for the LCD scenario. On average, the total change in the emissions of SO_2, NO_x, CO, VOCs, PM_{10} and $PM_{2.5}$ during LD-I lockdown period were −26%, −47%, −39%, −57%, −61%, and −46%, respectively. Moreover, VOCs emissions from sources of household solvent usage and hospital solvent usage increased by 30% in their estimation. More details can be found in a previous study by Li et al. (2020).

2.3. Process analysis of ozone formation

Being cognizant of the various complex chemical and physical processes interactions involved in O_3 formation, we activated the PA functionality within CMAQ in all our simulations to account for (and distinguish) the contributions of emissions, chemistry, transport and deposition processes while computing pollutant concentrations (Gonçalves et al., 2009). Essentially, we analyzed the hourly integrated process rate (IPR) contributions of gas-phase chemistry (CHEM), cloud and aqueous processes (CLDS), dry deposition (DDEP), vertical advection (ZADV), vertical diffusion (VDIF), horizontal advection (HADV), and horizontal diffusion (HDIF). Several studies have previously utilized and demonstrated the effectiveness of PA in explaining O_3 formation over YRD (Li et al., 2012; Lu et al., 2020; Ni et al., 2020; Shu et al., 2016; Wang et al., 2022a).

2.4. O_3-precursor sensitivity analysis based on HDDM-3D

Sensitivity analysis provides an estimate of the impacts caused by changes in emissions (or any other parameter) on ambient concentrations of atmospheric pollutants, and is a widely used approach to support air quality decisions and to inform effective emission control strategies (Clappier et al., 2017; Cohan and Napelenok, 2011). In this study, a detailed O_3-NO_x-VOCs sensitivity analysis is performed with CMAQ-HDDM-3D tool. The sensitivity coefficients of O_3 to NO_x and VOC emissions were calculated as follows:

$$S^{(1)} = E_0 \frac{\partial C}{\partial e} = E_0 \frac{\partial C}{\partial [(1+\Delta\varepsilon)E_0]} = \frac{\partial C}{\partial \varepsilon} \quad (1)$$

$$S^{(2)} = E_0 \frac{\partial}{\partial e}\left(E_0 \frac{\partial C}{\partial e}\right) = \frac{\partial^2 C}{\partial \varepsilon^2} \quad (2)$$

where $S^{(1)}$ and $S^{(2)}$ are the first- and second-order sensitivity coefficients, respectively. ε is a scaling variable of the emission of NO_x or VOCs, hence both the sensitivity coefficients and concentration have same units. Therefore, if for instance $S^{(1)}$ is equal to +α ppb (-α ppb), it implies that with a +10% perturbation in NO_x (or VOC) emissions, the concentration of O_3 would change by + 0.1α ppb (−0.1α ppb). Similarly, if

for instance $S^{(2)}$ is equal to +β ppb (-β ppb), it implies that with a +10% perturbation in NO_x (or VOC) emissions, instance $S^{(1)}$ would change by +0.1β ppb (−0.1β ppb).

Here, to quantify the impacts of the lockdown emission reductions on O_3 we utilized both the first- and second-order O_3 sensitivities with respect to NO_x and VOCs based on the Taylor series expansions (Eq. (3)):

$$C_{P(e=E_0+\Delta\varepsilon.E_0)} \approx C_{0(e=E_0)} + \Delta\varepsilon.S^{(1)} + \frac{(\Delta\varepsilon)^2}{2}.S^{(2)} \quad (3)$$

C_p is the pollutant concentration (i.e., O_3 in this study) after a fractional perturbation (Δε) in the emissions (e) of either NO_x or VOCs. The fractional perturbation (Δε) is the change of scaling variable of the emission of NO_x or VOCs. E_0 and C_0 both represent the normal or business-as-usual emissions and concentrations, respectively. With this, we rapidly determined the extent of O_3 increases due to the emission reductions of VOCs and/or NO_x at each grid cell over the YRD region, which facilitated a better understanding of the impact of emission controls on O_3 concentration over the YRD region. A detailed description of the structure, equations of sensitivity of O_3 to its precursors can be found in previous study by (Wang et al., 2022b).

2.5. Model performance assessment

This study utilized the same WRF input files used by Li et al. (2020), and the meteorological predictions covering the study period for this work have been well evaluated therein. In brief, the WRF predictions were found to be generally consistent with ground measurements, although there was a slight disagreement (negative bias) in the prediction of relative humidity. For the CMAQ model performance, the hourly simulated O_3 and NO_2 concentrations were compared with ground-based observations between 6 January to February 24, 2020, which adequately covers the period before (PLD) and during the lockdown (LD-I) over the YRD region. The ground measurements during this period were obtained from all the monitoring stations in all the 41 major cities across the YRD region, while the model simulations are average values at the grid cells corresponding to each monitoring station. We pay particular emphasis to the model performance results in the four key representative (capital) cities of Shanghai, Hangzhou, Nanjing and Hefei (Fig. 1). The results of the simulation-observation comparisons and statistical evaluation for both O_3 and NO_2 during the study period are summarized in the Supplementary Information (SI). Even with the slight under predictions, the CMAQ model captured relatively well the overall trend of O_3 and NO_2 during the study period, including the conspicuous increases that were observed during the COVID-19 lockdown period. Furthermore, as shown in Text S2 in the supplementary information our model performance results were largely comparable with previous studies (Liu et al., 2021; Wang et al., 2021, 2022a). Therefore, the CMAQ outputs for this study can therefore be utilized objectively for a detailed analysis of O_3-precursors relationship and to understand the O_3 increases observed during the lockdown period over the YRD region.

2.6. Data sources

To understand the spatial and temporal distribution of O_3 during the study period, we used ground measurements collected from all the 223 national monitoring sites in the 41 major cities within YRD (Fig. 1). These observations are archived at a repository maintained by the Ministry of Ecology and Environment of the People's Republic of China (http://datacenter.mep.gov.cn). Additionally, owing to the general lack of observations for VOCs over the YRD region, we obtained continuous measurements from 8 January to March 31, 2020 collected at a typical urban location in Changzhou city in the central of YRD, which adequately cover the period considered in this study. The methodology and processes involved in VOC data collection have been well covered in detail elsewhere (Zhang et al., 2022). For meteorological observations, we utilized hourly data from the weather monitoring sites in the 41 cities over YRD provided by the China Meteorological Administration (CMA: https://data.cma.cn/).

3. Results and discussion

As mentioned previously, a number of studies illustrated generally consistent changes in air quality over the YRD with regards to the lockdown restrictions (Huang et al., 2020; Li et al., 2020; Lian et al., 2020; Miyazaki et al., 2020; Pei et al., 2020; Shi and Brasseur, 2020; Wang et al., 2020b). Li et al. (2020) found that apart from O_3, the average concentrations of $PM_{2.5}$, PM_{10}, CO, NO_2 and SO_2 before (during) the lockdown reduced in 2020 by 12.3% (31.8%), 19.6% (33.7%), 7.8% (20%), 18.5% (45.1%) and 29.3% (20.4%), respectively, compared to similar period in 2019. The most puzzling change (and which is significant to our current study) relates to the significant increase of O_3, while its main precursors (e.g., NO_x) reduced substantially (Li et al., 2020; Liu et al., 2021; Zhao et al., 2020; Zhu et al., 2021). Text S1, Fig. S1 and Table S2 in the SI describes an overview of the evolution pattern and changes of O_3, NO_x and VOCs based on ground observations during PLD and LD-I periods juxtaposed with similar period in the previous three years (2017–2019 average). Here, we undertake a deeper exploration of these O_3 concentration changes before and during the lockdown period over the YRD region.

3.1. O_3 increases over YRD during COVID-19 lockdown

Fig. 2 shows the comparison of the daytime (9:00–16:00 local time, LT) concentrations of O_3 observations alongside the simulated concentrations for both the "BAU" and "LCD" scenarios averaged for all the national control monitoring stations in each of the key representative cities of Shanghai, Nanjing, Hangzhou and Hefei. We noted obvious increases of daytime O_3 during LD-I period relative to PLD (Fig. 2a), and the lowest and highest relative changes of observed ("BAU", "LCD") were about 43.9 (14.6, 67.1)% in Shanghai and 82.5 (49.1, 83.3)% in Hefei, respectively (Fig. 2b). Furthermore, as a result of the emission reductions during LD-I, highest daytime O_3 concentration increases occurred in Shanghai (24.2 μg/m^3), followed by Hangzhou (17.6 μg/m^3), Nanjing (16.6 μg/m^3) and Hefei (12 μg/m^3) (Fig. 2c). As expected, because Shanghai is a much larger city with intense emissions of O_3 precursors (especially NO_x), the impact of the COVID-19 lockdown controls on O_3 is certainly relatively higher than in the other key cities. This certainly shows that the control measures implemented during LD-I had significantly higher impact on O_3, and our results are generally consistent with other related studies that found closely similar O_3 increases during COVID-19 lockdown over the YRD region (Liu et al., 2020, 2021; Wang et al., 2022a).

3.2. Process analysis of ozone formation during the COVID-19 lockdown

Different atmospheric processes played an important role in O_3 formation during the lockdown period. This includes the net effect of chemistry, transport, and deposition processes. We noted that for both the BAU and LCD scenarios gas-phase chemistry (CHEM), vertical transport (VERT=VDIF + ZADV), dry deposition (DDEP), and to some extent horizontal transport (HORT=HADV + HDIF) were generally the dominant processes that can explain the spatiotemporal evolution pattern (including the removal or increases) of O_3 during the lockdown period over the YRD region. The aqueous and clouds chemistry contribution (not shown) had nearly negligible contribution to O_3 during the study period and was not included in our analysis. As shown in Fig. 3, CHEM and DDEP were the major process that consumed O_3 (indicated by negative magnitudes) especially in the urbanized areas of YRD, whereas VERT (dominated by positive magnitudes of VDIF) largely contributed in compensating and balancing off the O_3 losses.

Moreover, other than the widely varied contribution of HORT

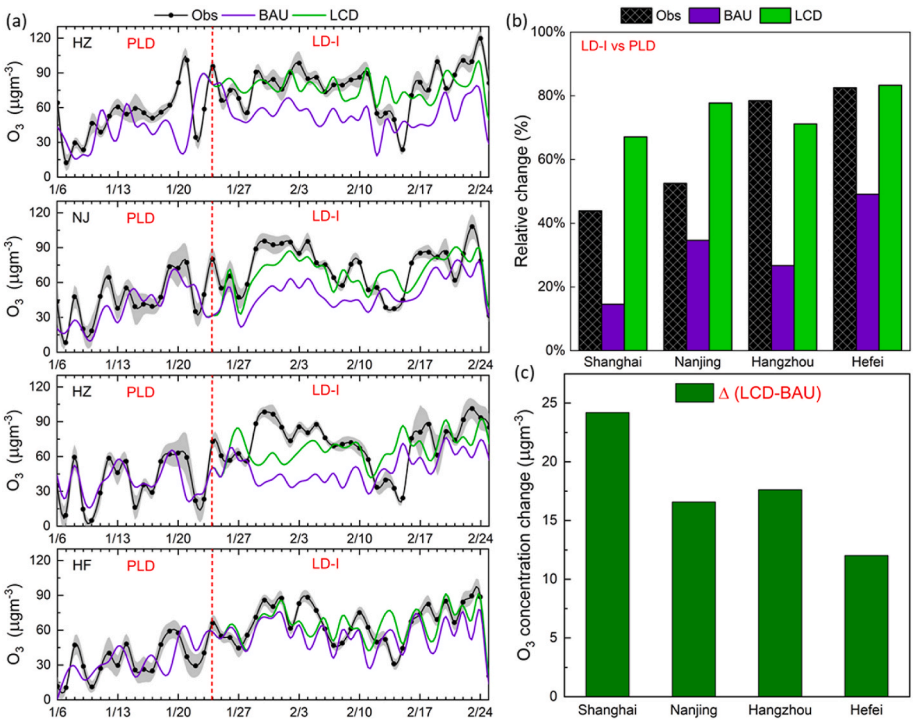

Fig. 2. (a) Daily variation of daytime averaged (9:00–16:00 LT) O_3 observations compared with the modeled "BAU" and "LCD" scenarios during PLD and LD-I in 2020 averaged at all the national control sites in Shanghai (SH), Nanjing (NJ), Hangzhou (HZ) and Hefei (HF). **(b)** Changes in observed and modeled daytime O_3 concentration during LD-I compared with PLD, and **(c)** averaged relative changes (LCD-BAU) during LD-I show the impact of COVID 19 lockdown on O_3. The red dashed line defines the pre-lockdown period (PLD) between 6th to 23rd January and lockdown Level I control period (LD-I) 24th January to 24th February 2020.

(dominated by HADV) to O_3 in different areas of YRD (see Fig.S4a in the SI), CHEM and VDIF exhibited higher magnitudes under the BAU scenario (Fig. 3a), which significantly reduced under the LCD scenario (Fig. 3b). Save for the slight increase in DDEP, the most notable IPR difference relates to the significant reduction of CHEM contribution that occurred primarily in the eastern and centrals areas of YRD where O_3 concentration increases were highest (Fig. 3c). This includes the most urbanized cities of Ningbo, Hangzhou, Shanghai, Suzhou and Nanjing among others. Because these cities are inherently within the most developed core region of YRD where intense emission of O_3-precursors from anthropogenic sources is usually prevalent (An et al., 2021), it then means that the lockdown restrictions directly lowered the capacity of chemical consumption of O_3 via NO-titration due to the substantial reduction of NO_x emissions during LD-I. These findings are generally consistent with previous studies (Li et al., 2020; Wang et al., 2020a, 2022a). However, although there was an increase in DDEP during LD-I, the enhancement was too little to balance off the much higher reduction in CHEM (Fig. 3c). Furthermore, the daytime CHEM contribution to odd oxygen (CHEM-O_x) hardly exceeded 5 μg/m^3 for both simulation scenarios, but instead it exhibited a general reduction under the LCD scenario even in areas that exhibited higher O_3 increases as shown in Fig. S4b in the SI.

From a temporal perspective (Fig. 4 and Fig. S5), the simulated O_3 concentrations exhibited a typical diurnal pattern during LD-I: low levels in the early morning hours, followed by a steady increase during mid-morning, before peaking in the afternoon, and thereafter declining gradually to low levels in the evening. As shown in Fig. 4, the lowest O_3 concentrations and the conspicuously pronounced negative CHEM contribution occurred between 6:00–8:00 LT and from around 18:00–19:00 LT, which is mainly the result of the combined effects of diurnal changes in meteorological conditions (such as changes in the height of the boundary layer, changes in radiation intensity) and diurnal changes in emissions.

Between 9:00–16:00 LT CHEM contribution to O_3 weakened, whereas CHEM-O_x as well as O_3 concentrations increased correspondingly (Fig. 4). This pattern between CHEM-O_x and O_3 concentration was also similar at the rural sites (Fig. S5). However, compared to the urban locations, the IPR magnitudes were significantly lower and relatively the same between the BAU and LCD scenarios at the rural sites. Moreover, other than the rural SFM site, dry deposition was the main sink for O_3 in the other typical rural sites in addition to the dismal contribution of CHEM. Logically, there is an overall lower emission of NO_x in rural locations than in urban areas, hence the obvious lower impact of O_3 consumption through NO-titration.

The vertical profile of IPR outputs is shown in Fig. 5. We note that within the atmospheric boundary layer (ABL: i.e. modeling layer 1–8 in this study), the variation of the magnitudes of the main processes contributing to O_3 formation and removal were higher at the surface than in the upper layers. Gas-phase chemistry continued to significantly consume O_3 from the surface to about layer 5 (~350 m above ground level), while both vertical and horizontal transport processes not only balanced off the O_3 loss through CHEM but led to additional O_3 especially over most of the urban atmosphere. Notably, as height above the ground surface increased in the urban areas, and at higher altitude the contribution of CHEM and VERT processes diminished and became increasingly positive and negative, respectively (Fig. 5). For instance, at the urban sites in Shanghai (JA), Hangzhou (WB), and Hefei (MS) cities, the contribution of chemistry to ozone transitioned to being positive (albeit with a small magnitudes) beyond ~500 m, ~160 m and ~240 m above the ground level respectively (Fig. 5). At the suburban DSL (in Shanghai) and DPR (in Hefei) the negative chemical contribution was confined within ~160 m and ~90 m, respectively, whereas at the rural QDL site, chemistry contributed positively from the surface to more 2 km above the surface (Fig. S6). This means that at upper layers towards the top of the ABL, gas-phase chemistry (though dismal) contributed positively to O_3 production, and the O_3 formed was then transported downwards via VDIF. It is understandable that solar radiation is relatively higher at such high altitudes, which create more favourable conditions for photochemical reactions, and which could yield more O_3 than at the surface. At the rural sites, the first layer revealed the only significant magnitudes of IPR outputs (Fig. S6), which were still much lower than in the urban locations. Overall, whether at the urban or rural sites, the magnitudes of most dominant processes that contributed to O_3 during LD-I were much higher at (or near) the surface for both scenarios,

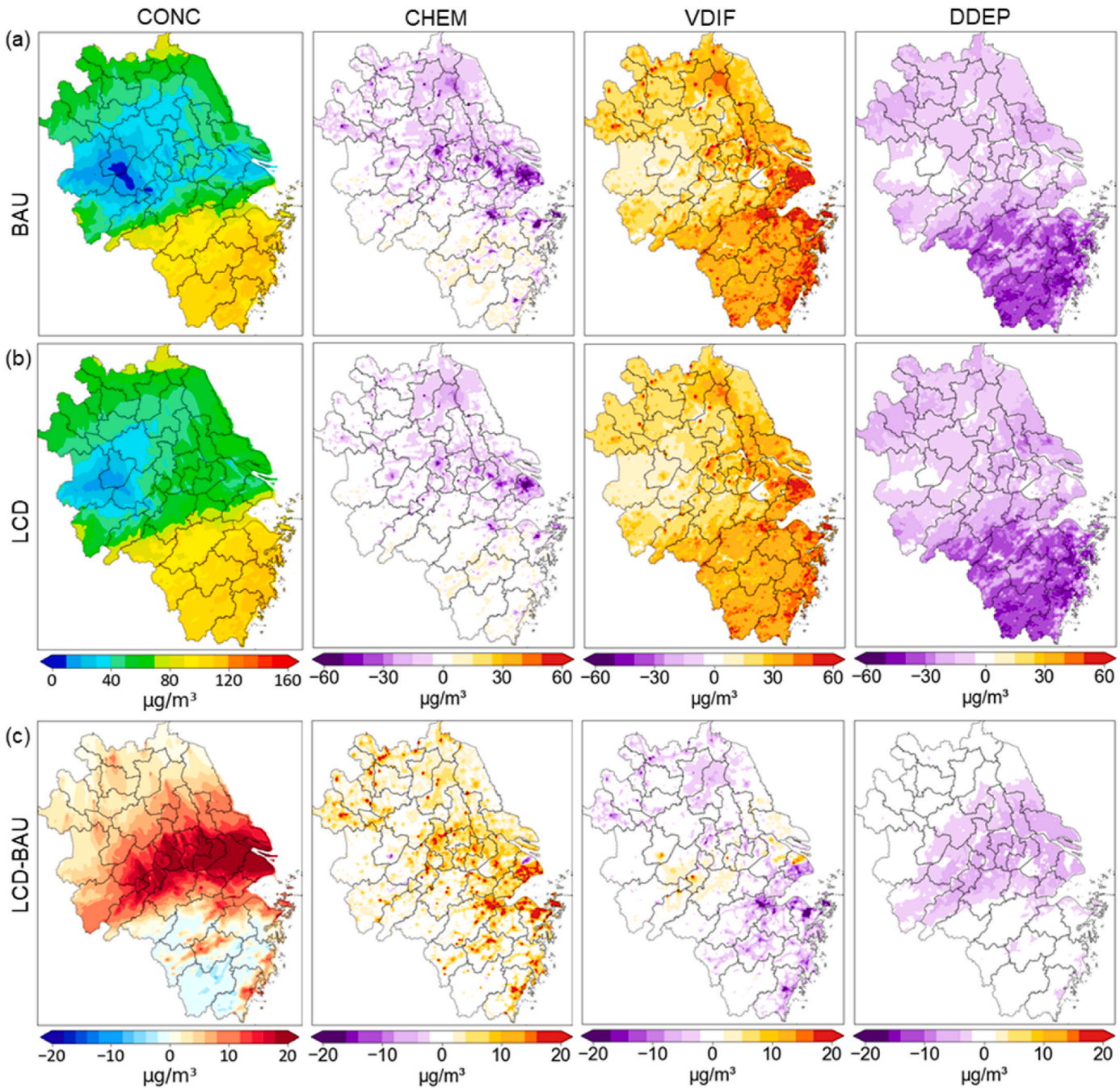

Fig. 3. Spatial distribution of simulated daytime (9:00–16:00 local time) average ground-level O_3 concentration (CONC) and their corresponding contributions from gas-phase chemistry (CHEM), vertical diffusion (VDIF) and dry deposition (DDEP) over the YRD region during LD-I period. (**a**) Represent BAU scenario, (**b**) is for LCD scenario and (**c**) is the difference between LCD and BAU. (LD-I is the COVID-19 lockdown period between 24th Jan.-24th Feb 2020).

which could explain the much wider gap and lower levels of O_3 concentration at the surface than at higher altitudes. This also indicates that the emission reduction measures during the lockdown period had a significant impact on the chemistry and ultimate formation of O_3 at the surface.

For a closer look at Figs. 3, Figs. 4 and 5, the BAU scenario exhibited larger IPR magnitudes and lower O_3 levels, while the LCD scenario showed significantly reduced IPR magnitudes and substantial increase in O_3 levels. To understand the scale of these changes, we computed the differences between the two scenarios at both the urban and rural sites as shown in Table 1. Among the urban and rural/suburban sites the highest changes in O_3 (CHEM, VERT) of about 22.75 (−20.2, −17.3) μg/m^3 and 13.96 (−12.4, −10.9) μg/m^3 occurred at Shanghai-JA (among the urban sites) and SFM (among the rural sites), respectively. On the other hand, lowest changes of about 12.10 (−13.5, −10.7) μg/m^3 and 5.41 (−0.67, −0.81) μg/m^3 were prevalent at the urban Hefei-MS and at the rural QDL sites, respectively. These relatively low changes generally reflect the lower intensity of O_3-precursor emissions, which is synonymous of the obvious lower contribution of the main IPR variables to the O_3 levels at these sites.

As mentioned previously, the combined decrease of VERT and the enhancement of DDEP still didn't balance off the higher decline of CHEM contribution during LD-I. For instance, in the urban sites of Shanghai, Hangzhou, Nanjing and Hefei the change in CHEM (VERT, DDEP) was about −20.2 (−17.3, 0.03) μg/m^3, -16.8 (−13.4, 1.37) μg/m^3, -12.2 (−9.71, 1.67) μg/m^3 and -13.5 (−10.7, 1.31) μg/m^3,

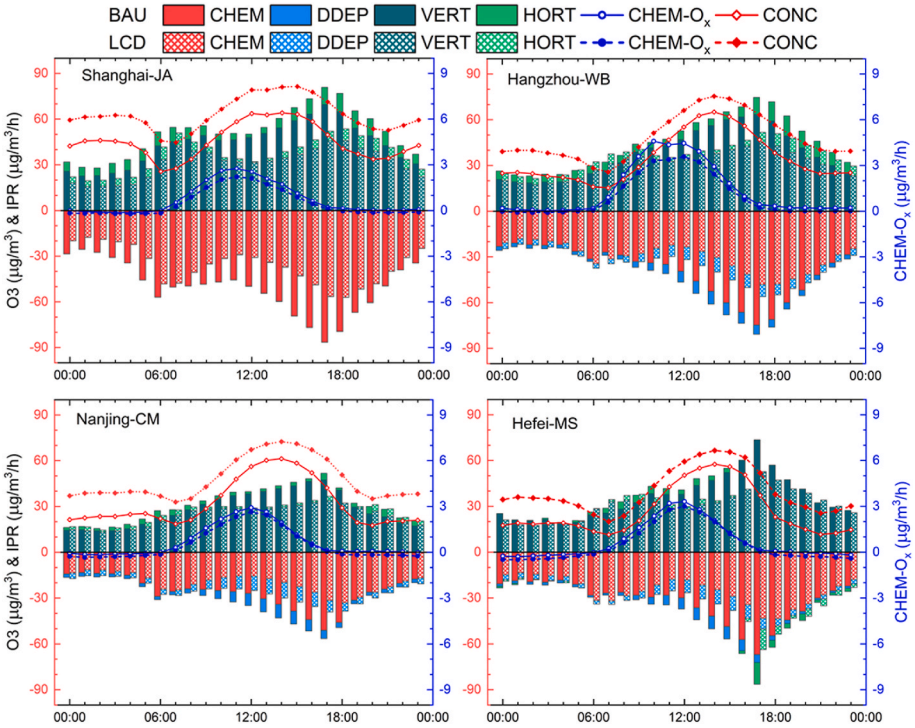

Fig. 4. Diurnal variations of O_3 concentrations and the main atmospheric processes contributions at the surface layer (0–40 m) for the BAU and LCD scenario during LD-I at typical urban locations in Shanghai, Hangzhou, Nanjing and Hefei. (CHEM: gas-phase chemistry; DDEP: dry deposition; VERT: vertical transport, i.e. the net effect of ZADV and VDIF; HORT: horizontal transport, i.e. the net effect of HADV and HDIF; CHEM-O_x: gas-phase chemistry contribution to O_x; CONC: average O_3 concentration). LD-I is the COVID-19 lockdown period between 24th January-24th February 2020.

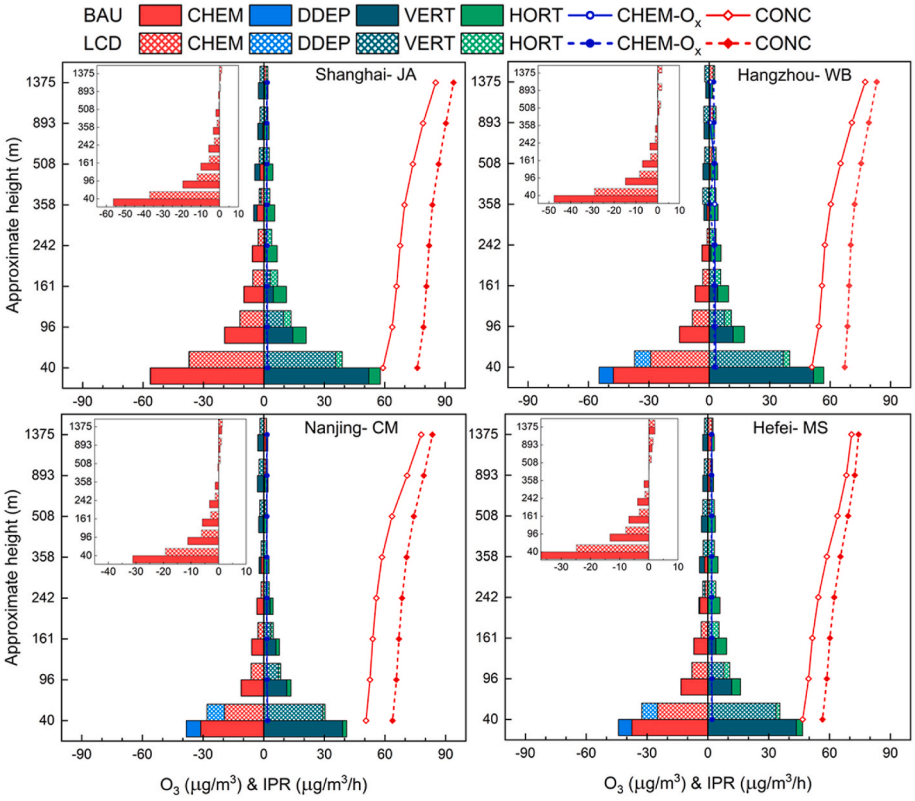

Fig. 5. Vertical profile of simulated daytime average (09:00–16:00 LT) O_3 concentration and the main atmospheric processes contributions under the BAU and LCD scenarios during LD-I for the model layers 1–8 at typical urban sites in Shanghai, Hangzhou, Nanjing and Hefei. (CHEM: gas-phase chemistry; DDEP: dry deposition; VERT: vertical transport, i.e. the net effect of ZADV and VDIF; HORT: horizontal transport, i.e. the net effect of HADV and HDIF; CHEM-O_x: gas-phase chemistry contribution to O_x; CONC: average O_3 concentration). The inset figures show the vertical profile of CHEM contribution. The approximate height of each model layer is as defined in Table S9. LD-I is the COVID-19 lockdown period in YRD region between 24th January-24th February 2020.

respectively (Table 1). This indicates that the substantial changes in gas-phase chemistry (unlike transport and deposition processes) could sufficiently explain the possible impact of O_3-precursors reductions on O_3 formation during the lockdown period. Actually, since negative CHEM contribution is inherently tied to the consumption of O_3 via the NO_x-titration effect, the changes in IPR budget suggests that the reduction of anthropogenic NO_x emissions during the COVID-19 lockdown didn't lead to a fast chemical production of O_3, but rather potentially contributed to a 42.9%, 33.5%, 32.8% and 26% O_3 increase in Shanghai-JA, Hangzhou-WB, Nanjing-CM and Hefei-MS, respectively (Table 1). These results are supported by the work of Wang et al. (2022a) that found significant decrease (increase) of chemical production (loss) of O_3

Table 1
The relative changes between the LCD and BAU scenarios of the daytime average (9:00–16:00 LT) surface O_3 concentration and the corresponding atmospheric processes contributions during LD-I period between 24th Jan.-24th Feb 2020 at typical urban (Jing'an: JA; Wolong bridge: WB; Caochangmen: CM and Mingzhu square: MS) and rural sites over the YRD region (Dianshan Lake (DSL), Qiandao Lake (QDL), Dongpu Reservoir (DPR) and Shangfang Mountain (SFM)).

Variable[a]		CONC		CHEM		CHEM-O_x		DDEP		VERT		HORT	
Change[b]		μg/m^3	%	μg/m^3	%	μg/m^3	%	μg/m^3	%	μg/m^3	%	μg/m^3	%
Urban Sites	JA	22.75	42.9	20.2	−35.8	−0.40	−20.0	−0.03	20.6	−17.3	−33.2	−2.59	−45.4
	WB	17.08	33.5	16.8	−36.6	−0.74	−22.3	−1.37	20.5	−13.4	−26.7	−1.87	−37.4
	CM	16.74	32.8	12.2	−39.2	−0.23	−11.7	−1.67	23.3	−9.71	−24.9	−0.72	−36.0
	MS	12.10	26.0	13.5	−35.9	−0.23	−10.5	−1.31	20.0	−10.7	−24.4	−1.22	−39.4
Rural Sites	DSL	12.08	17.5	3.75	−47.3	−0.14	−10.1	−1.57	19.4	−2.76	−14.3	0.52	−38.3
	QDL	5.41	9.7	0.67	47.6	−0.24	−8.2	−0.91	7.3	−0.81	−5.1	0.32	−38.6
	SFM	13.96	22.6	12.4	−37.9	−0.53	−24.1	−0.03	19.6	−10.9	−33.3	−1.19	−74.8
	DPR	8.16	15.5	3.36	−49.8	0.31	14.6	−1.22	15.0	−2.25	−12.9	0.004	−6.9

[a] CONC: averaged concentrations of O_3; CHEM: gas-phase chemistry; CHEM-O_x: gas-phase chemistry contribution to O_x; DDEP: dry deposition; VERT: vertical transport, i.e., the net effect of ZADV and VDIF; HORT: horizontal transport, i.e., the net effect of HADV and HDIF.
[b] Change (μg/m^3) = LCD-BAU; Change (%) = ((LCD-BAU)/BAU) *100.

because NO_x reductions during lockdown shrunk the NO-titration effect, and hence resulting in an increase of O_3 concentration.

Moreover, as shown in Table 1, contrary to O_3 concentration increases, the changes in CHEM-O_x during LD-I were about −0.40 μg/m^3 (−20%), −0.74 μg/m^3 (−22.3%), −0.23 μg/m^3 (−11.7%) and −0.23 μg/m^3 (−10.5%) in the urban sites of Shanghai-JA, Hangzhou-WB, Nanjing-CM and Hefei-MS, respectively. Similar change of CHEM-O_x of about 0.14 μg/m^3 (−10.1%), −0.24 μg/m^3 (−8.2%) and −0.53 μg/m^3 were noted at the rural sites of DSL, QDL and SFM, respectively, except a slight increase of about 0.31 μg/m^3 (14.6%) at the DPR site (Table 1).

The IPR results above highlight critical links of emission reductions (especially for NO_x) to the increases in O_3 during the lockdown period, which could be a key issue for wintertime air quality management over YRD. To have a better understanding of this challenge, we conducted comprehensive investigation of O_3-pecursors sensitivities during LD-I using the CMAQ-HDDM-3D tool. We focused on probing the changes of 1st- and 2nd-order sensitivities of O_3 to its precursors, and the role of emissions reductions on the dominant chemical regimes of O_3 formation during LD-I. This allows for a broader assessment of the extent to which O_3-precursor reductions contributed to the significant O_3 increases during the lockdown period, which could eventually have positive implications to O_3 control over the YRD region.

3.3. O_3-NO_x-VOCs sensitivities during COVID-19 lockdown

Fig. 6 shows the variation of domain-wide first-order sensitivities of O_3 to AVOCs (anthropogenic VOCs) (S^1_{AVOC}) and NO_x ($S^1_{NO_x}$), as well as the second-order derivatives to NO_x ($S^2_{NO_x}$) during LD-I period. Here, we quantified the O_3-precursors sensitivities that represent the daytime (9:00–16:00 LT) O_3 concentration for both BAU and LCD simulations. As noted previously (and as shown in Fig. 6), O_3 concentration under the LCD scenario was generally higher than that of the BAU scenario, and the increase was largest in the middle part of the YRD region. For example, the increase of O_3 concentrations in Shanghai, Changzhou, Wuhu, Hefei, etc. was close to or exceeded 20 μg/m^3. Notably, almost all sensitivities had lower magnitudes under the BAU scenario (Fig. 6a), compared to the significantly high value under the LCD scenario (Fig. 6b). Specifically, S^1_{AVOC} barely exceeded 10 μg/m^3 over the YRD domain during LD-I with a slight change of about 2–4 μg/m^3 between the BAU and LCD scenarios along the coastal cities and some areas in central YRD within Jiangsu province (Fig. 6c). Although S^1_{AVOC} increases were generally prevalent in the areas where O_3 exhibited increased concentration, the increases of these (S^1_{AVOC}) sensitivities in the central areas of YRD region consisting of highest O_3 increases were moderate. Meanwhile, since the second-order O_3 sensitivities with respect to AVOC emissions were largely 'zero' for both scenarios, it indicated that O_3 response to changes in AVOCs emissions is basically linear. Thus, it can be concluded that reduction measures targeting key sources of AVOC emissions would yield positive effect to O_3 mitigation over YRD. This is consistent with previous studies (Wang et al., 2022a; Zhang et al., 2022).

In both the BAU and LCD scenarios, $S^1_{NO_x}$ was negative, which means that the reduction of NO_x emissions would obviously lead to an increase in O_3 concentration. Compared with the BAU scenario, the magnitudes of $S^1_{NO_x}$ in the LCD scenario were significantly larger. Interestingly, compared with the BAU scenario, the areas that displayed the highest O_3 increases also showed significant enhancement of both $S^1_{NO_x}$ and $S^2_{NO_x}$ under the LCD scenario, particularly within the central areas of YRD. These areas represent the core of YRD region with high concentration of industrial activities, power plants and vehicles that emit high levels of NO_x, resulting in the significant response of O_3 to changes in these emissions. Consequently, due to the COVID-19 lockdown the magnitudes of $S^1_{NO_x}$ and $S^2_{NO_x}$ were significantly enhanced, and the enhancement effect was very evident in the central areas of the YRD region where O_3 increases were most prominent. Therefore, anthropogenic emission reductions during COVID-19 lockdown led to the stronger first-order O_3-NO_x sensitivities (that were largely negative and farther away from zero), as well as much stronger second-order O_3 sensitivities to NO_x (that were generally positive and also farther away from zero). In short, the first- and second-order sensitivities of O_3 to NO_x were intensified from the BAU scenario to the LCD scenario, presenting a convex response pattern between O_3 concentrations and NO_x emission. In other words, the reduction in NO_x emissions during the COVID-19 lockdown not only caused an increase in O_3 concentrations, but also an increase in the absolute value of the sensitivity of O_3 concentration to NO_x emission.

At the grid cells corresponding to the selected typical sites, O_3 under the LCD scenario displayed evidently higher sensitivities, and in both scenarios the magnitudes of $S^1_{NO_x}$ and $S^2_{NO_x}$ were much larger than S^1_{AVOC} (Fig. 7a). For instance, the absolute changes of daytime average (9:00–16:00 LT) S^1_{AVOC} ($S^1_{NO_x}$; $S^2_{NO_x}$) at the urban JA, WB, CM and MS were 1.0 (7.7, 18.4) μg/m^3, 2.8 (9.0, 23.4) μg/m^3, 1.9 (11.0, 17.2) μg/m^3 and 1.7 (7.8, 15.7) μg/m^3, respectively (Fig. 7B left). Similarly, S^1_{AVOC} ($S^1_{NO_x}$; $S^2_{NO_x}$) at the typical rural sites DSL, QDL, SFM and DPR changed by 2.6 (14.8, 26.9) μg/m^3, 4.8 (17.4, 6.1) μg/m^3, 2.9 (13.3, 34.7) μg/m^3 and 3.0 (10.6, 19.7) μg/m^3, respectively (Fig. 7b right). Overall, the LCD (compared to the BAU) scenario revealed that during LD-I period, S^1_{AVOC} almost doubled; $S^1_{NO_x}$ widened by about a third; and $S^2_{NO_x}$ tripled on average at both the typical urban and rural areas of YRD. Although we noted a considerable enhancement of O_3-VOC sensitivities, these results indicated that O_3 was actually more sensitive to the changes in NO_x emissions during the lockdown period over YRD region, which is also consistent with previous studies (Liu et al., 2020; Wang et al., 2022a). Our findings present a rather straightforward and more elaborate understanding of the inherent changes in O_3-NO_x-VOC interactions during

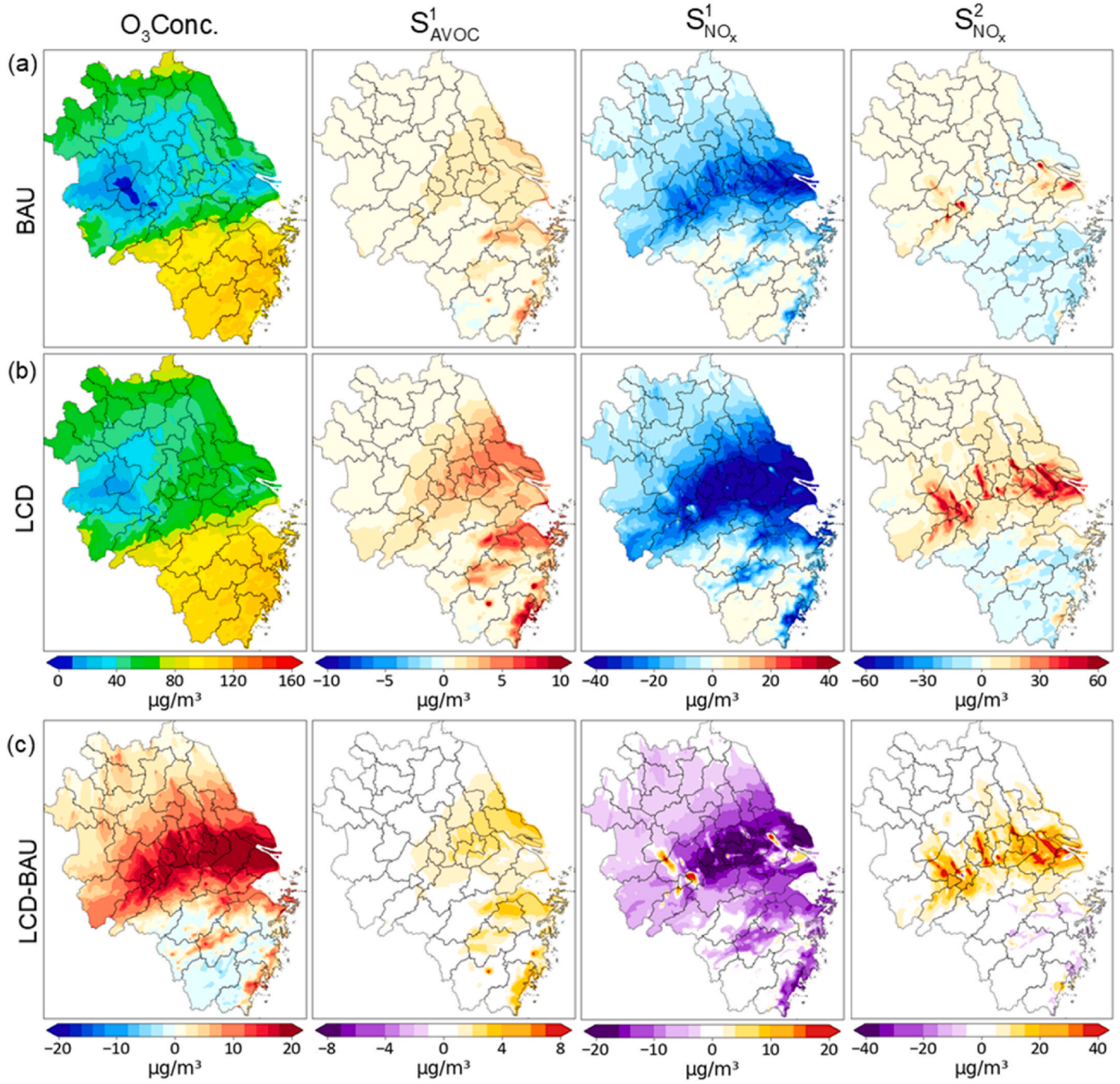

Fig. 6. Spatial distribution of simulated O_3 concentration and the corresponding sensitivities with respect to NO_x and AVOC emissions for the (**a**) BAU scenario, (**b**) LCD scenario and (**c**) changes during LD-I period over the YRD. The values are average for the daytime hours between 9:00–16:00 local time during the lockdown period between 24th Jan.-24th Feb 2020.

the lockdown, and which provides a reasonable explanation for the observed O_3 increases. Besides, our results highlight critical aspects of O_3-precursor responses in the YRD region, hence forms a strong basis for assessing O_3 control strategies over the region

It should be noted that non-zero magnitudes and signs of the second-order sensitivities have been previously utilized to indicate whether a pollutant-precursor relationship is linear or nonlinear (Wang et al., 2022b). In fact, the larger the second-order sensitivity coefficients the greater the nonlinearity, and a matched (or unmatched) signs of the first- and second-order sensitivity coefficients signify a concave (or convex) nonlinear relationship (Arter and Arunachalam, 2021). As shown in both Figs. 6 and 7, O_3 response to NO_x emissions under both simulation scenarios displayed contrasting magnitudes of $S^1_{NO_x}$ (negative) and $S^2_{NO_x}$ (positive), which were larger under the LCD scenario, and which could be the key reason behind the O_3 increases during the lockdown period. Besides, this significant variation of $S^1_{NO_x}$ and $S^2_{NO_x}$ during LD-I generally highlighted a convex O_3-NO_x response synonymous to the widely known "NO_x disbenefit" phenomenon. This is a typical characteristic feature of nonlinear chemistry of O_3-precursors formation associated with a reduced NO-titration rate, which has been applied extensively to explain the reason for the higher O_3 concentrations during weekends (i.e. "weekend ozone effect") when NO_x emissions are low (Fujita et al., 2016; Wang et al., 2014). For detailed understanding of these changes in O_3 responses to precursors we further

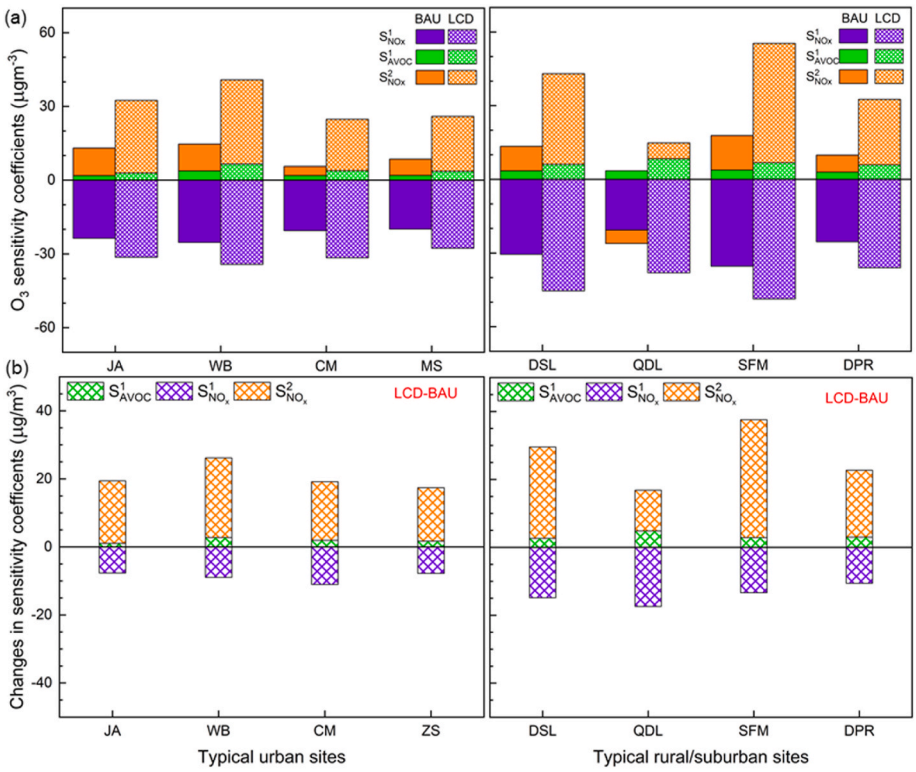

Fig. 7. Daytime (9:00–16:00 LT) average (**a**) O_3-NO_x-VOC sensitivities and (**b**) the difference between BAU and LCD scenarios during LD-I at the typical urban (left) and rural (right) locations. The LD-I is the COVID-19 lockdown period between 24th Jan.- 24th Feb 2020.

investigated the chemical regimes under which O_3 was formed during LD-I.

3.4. Ozone sensitivity regimes in YRD region during COVID-19 lockdown

We utilized the relationship between S^1_{AVOC} and $S^1_{NO_x}$ to describe the full range of O_3 sensitivity regimes during the lockdown period, we

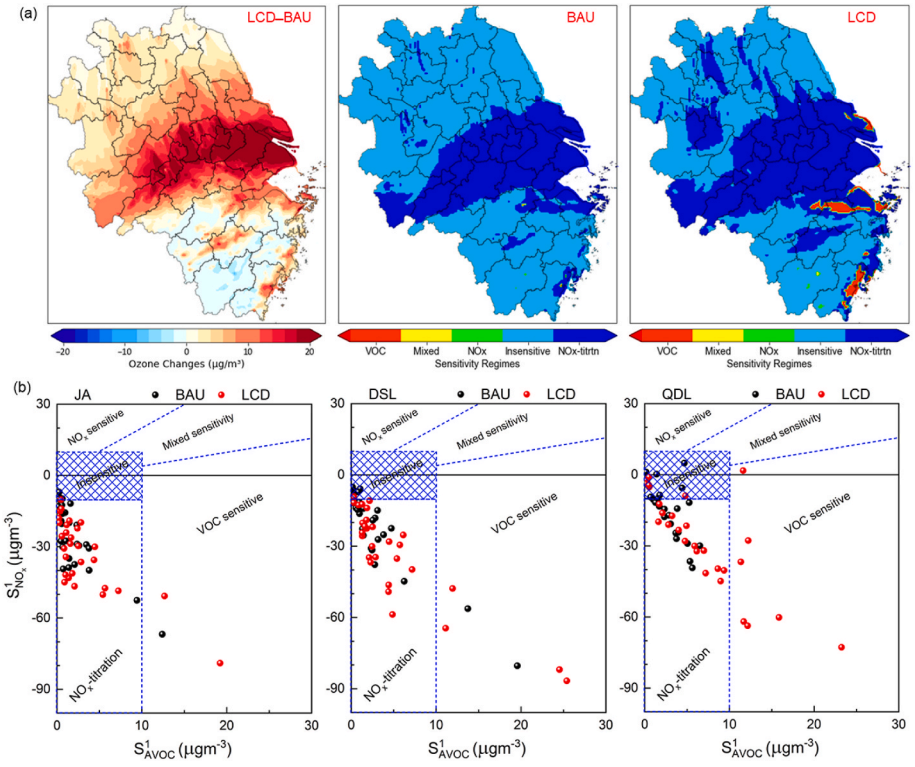

Fig. 8. (**a**) Spatial pattern O_3 concentration changes (left) and sensitivity regimes for the BAU (center) and LCD (right) scenario. (**b**) Scatter plots for the 1st-order O_3 sensitivity coefficients with respect to AVOCs (x-axis) and NO_x (y-axis) emissions for both the BAU (blue dots) and LCD (green dots) scenarios at the grid cells corresponding to typical urban JA (left), suburban DSL (center) and rural QDL (right) sites. The values are daytime average (9:00–16:00 LT) during LD-I period between 24th Jan. to Feb. 24th, 2020. The blue dashed lines in (B) identify the different categories of O_3 sensitivity regimes: VOC-sensitive, NO_x-sensitive, mixed sensitivity, NOx-titration and insensitive (shaded) regimes. The definition of the different categories of sensitivity regimes are found in (Wang et al., 2022b).

utilize definitions found a previous study by Wang et al. (2022b). Fig. 8 depict the different O_3 chemical regimes (i.e., VOC-sensitive, NO_x-sensitive, mixed-sensitivity, NO_x-titration and insensitive) over the YRD region and in selected typical sites during LD-I. Under both BAU and LCD scenarios, we generally noted that O_3 formation during LD-I predominantly occurred under insensitive and NO_x-titration regimes, and to a lesser extent VOC-sensitive conditions confined within specific localities (Fig. 8a). The insensitive regime dominated most of the northern and southern areas of YRD region, which signified that O_3 in these areas was typically influenced either by transport and/or boundary conditions rather than photochemical formation (Sillman and West, 2009). The clearly defined VOC-sensitive chemistry mainly occurred around the coastal cities of Wenzhou, Zhoushan, Ningbo, Shaoxing Hangzhou Bay area, Shanghai and Nantong. We previously indicated that these coastal cities host among the largest petrochemical industries and refineries that emit VOC emissions with obvious influence on O_3 formation. Furthermore, except for a few point sources in Lishui and Wenzhou we did not find locations where O_3 formation was dominated by NO_x- or mixed sensitivity conditions during LD-I (Fig. 8a).

Interestingly, we also noted that major increases of simulated O_3 during LD-I occurred in the areas that exhibited typical NO_x-titration conditions mainly in the eastern and central YRD (Fig. 8). These areas usually constitute the megacity clusters and other highly urbanized areas with intense O_3-precursor emissions. Therefore, the substantial reduction of these emissions (particularly NO_x) during the lockdown period led to a sharp decrease in the chemical titration of O_3 that expanded widely over larger areas, effectively exemplifying "the NO_x titration trap" phenomenon (Tang et al., 2021). Even at the grid cells corresponding to typical urban, suburban and rural sites of YRD, NO_x-titration regime dominated the daytime O_3 formation with a slight increase of VOC-sensitivity under the LCD scenario (Fig. 8b). Our findings are consistent with the studies that pointed out the prevalence of dominant NO-titration conditions during the lockdown period over the YRD region (Wang et al., 2020a, Wang et al., 2022a), but challenge other previous studies that reported the dominance of VOC-sensitive conditions (Liu et al., 2020; Wang et al., 2021).

The comprehensive diagnosis of O_3 chemical regimes above paves way for assessing the impact of O_3 control measures. Typically, measures targeting the reduction of AVOC, NO_x or both emissions are often most effective to control O_3 under VOC-, NO_x- or mixed-sensitivity conditions, respectively (Wang et al., 2022b). Otherwise, counter-productive outcomes that result in O_3 concentration increases could occur even with a fractional reduction of NO_x (or VOC) in the VOC- (or NO_x-) sensitive areas. Therefore, since the NO_x-titration regime was widespread during the lockdown period, and considering the significant enhancement of O_3-NO_x nonlinearity (discussed in previous section), it became necessary to assess the impact of NO_x and AVOC emission reductions under the prevailing conditions. This way, we can gain further insight to ascertain the extent to which O_3-precursors reductions would influence O_3 concentrations and understand why O_3 spiked during the lockdown period.

3.5. Implications for O_3 control measures

During winter, O_3 hardly causes pollution according to the present National Ambient Air Quality Standards of China, but the increase of O_3 concentration like those observed under the LCD scenario are usually accompanied by the change of O_3 formation mechanism. We utilized the S^1_{AVOC}, $S^1_{NO_x}$ and $S^2_{NO_x}$ to project the impact of a broader range of NO_x and VOC reductions on O_3 concentrations based on the Tylor series expansion (Eq. (3)). As shown in Fig. 9, the impact of NO_x reductions on daytime (9:00–16:00LT) O_3 changes is much profound compared to AVOC reductions. At both the typical urban and rural sites, NO_x reductions hinted at a significant disbenefit to O_3 control over YRD. We further noted that the projections based on first-order sensitivity alone displayed lower O_3 changes compared to those that included the second-order terms (Fig. 9). For instance, at the urban JA site in Shanghai, the projections based on $S^1_{NO_x}$ alone resulted in O_3 increases of about 3.9 μg/m^3, 11.6 μg/m^3 and 27.1 μg/m^3 with NO_x reductions of 10%, 30% and 70%, respectively (Fig. 9 left). On the other hand, at the same site projections based on both $S^1_{NO_x}$ and $S^2_{NO_x}$ led to O_3 increases of about 4.0 μg/m^3, 13.0 μg/m^3 and 34.6 μg/m^3 (Fig. 9 right), which was about 4%, 12% and 28% higher. This clearly shows that with higher NO_x

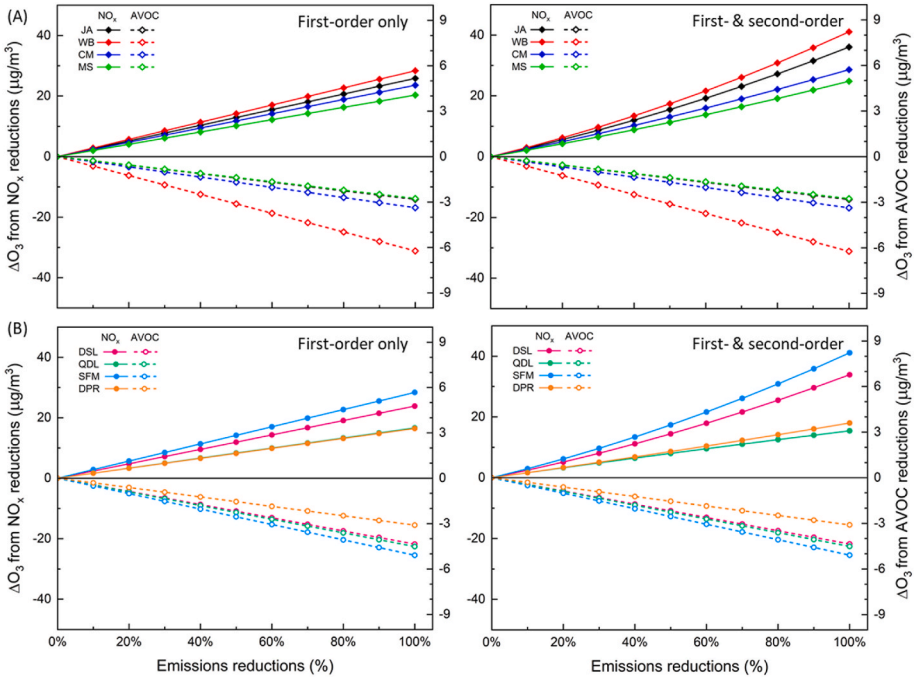

Fig. 9. Projections of daytime average (9:00–16:00 LT) ozone changes over typical (**A**) urban and (**B**) rural sites with respect to controlling a wider range of the anthropogenic emissions of either NO_x (solid lines) or VOCs (dashed lines). The values are based on the simulated O_3 first-order (left) and both first- and second-order (right) sensitivity coefficients from both the BAU and LCD scenarios during lockdown period between 24th Jan. to 24th Feb. 2020.

reductions nonlinearity would increasingly enhance and accelerate the rate of O_3 increase over the YRD region.

Therefore, in addition to the substantial weakening of the NO-titration effect it appears that the nonlinear relationship between O_3 and NO_x is also a critical issue that can explain the O_3 increases that occurred over YRD during the lockdown period. From these findings, we can recognize the usefulness of quantifying the higher- (second-) order sensitivities using the HDDM technique, so as to have a straightforward understanding of intrinsic O_3-precursors relationships that would have been otherwise overlooked by other sensitivity analysis approaches. With regards to the insignificant (mostly "zero") magnitudes of O_3 second-order sensitivity to AVOC emissions, the projections presented in Fig. 9 indicate that O_3 concentrations would obviously decrease linearly with respect to VOC reductions of over the YRD region. This therefore means an emission reduction strategy focusing on AVOCs emissions would yield positive benefits for wintertime O_3 decrease. This is supported by other previous studies that suggested prioritization of VOC reductions to decrease O_3 concentration over YRD during the winter season (Wang et al., 2022a). Although wintertime emissions of VOCs are usually lower, especially because of the negligible biogenic VOCs and fewer evaporative sources, targeted elimination of the potential VOC emission (as opposed to NO_x) sources especially in locations showing conspicuous VOC-sensitive chemistry would go a long way in mitigating possible O_3 increases during winter over the YRD region as indicated in this work.

4. Conclusions

In this work, detailed investigation of the changes in O_3-precursors sensitivity and integrated process rates was conducted with CMAQ-based HDDM and PA tools during the first month of COVID-19 lockdown period over the YRD region. Using simulations with (and without) developed anthropogenic emission inventory reflecting the lockdown (and "business-as-usual") conditions, we noted dramatic increase in daytime O_3 (about 10–43%) that coincided with a significant weakening of the contribution (negative) of gas-phase chemistry to O_3 (about 35–50%) over most areas in eastern and central YRD. Similarly, we also noted profound changes in O_3-NO_x-VOC sensitivities in the same areas consisting highest O_3 increases. Results showed generally negative (positive) magnitudes of first-order O_3 sensitivity to NO_x (AVOC) that were mostly lower than -20 μg/m^3 (lower than 10 μg/m^3) in the key cities of YRD including Shanghai, Hangzhou, Nanjing and Hefei. Most significantly, the O_3 precursors emission reduction during the lockdown highlighted substantial changes of both the 1st- and 2nd-order O_3 sensitivities with respect to the changes in NO_x emissions. Results show that the latter increased by about a factor of three following the emission reductions during the lockdown period. These changes in O_3-NO_x sensitivities not only indicated that O_3 formation during the lockdown period was largely more sensitive to NO_x than AVOCs emissions, but also the presence of a strong nonlinear and convex O_3 response to changes in NO_x emissions, which was indicative of a "NO_x reductions disbenefit" phenomenon. Besides, the concurrent manifestation of first-order sensitivities of O_3 to AVOC (less than 10 μg/m^3) and to NO_x (less than -10 μg/m^3) elucidated a clearly defined NO_x-titration regime that expanded considerably under the lockdown conditions.

What's more, because of the substantial changes of the 1st- and 2nd-order sensitivities of O_3 to NO_x emissions, results show that at the typical urban site in Shanghai for instance, the nonlinear relationship of O_3 with respect to 47% NO_x reductions under the lockdown scenario potentially contributed approximately 20% increase in O_3 concentration during the lockdown period. We have also shown that with higher NO_x reductions this nonlinearity would progressively enhance and accelerate the rate of O_3 increase over the YRD region.

Our findings generally highlighted fundamental insights regarding the significant changes of O_3-NO_x sensitivities following the emission reduction measures that occurred over YRD due to COVID-19 lockdown. In part, the results provide key insights into the underlying chemistry and nonlinear behavior of O_3 under relatively high NO_x reduction measures, which could be a useful hint for wintertime O_3 control strategy. From the simulated changes of both the 1st- and 2nd-order O_3-precursors sensitivities, our results suggest that efforts targeting VOC (NO_x) reduction could be a beneficial (detrimental) strategy to reduce O_3 concentrations during winter over the YRD region. We further note that with the growing improvement of emission inventories, the 1st-order and 2nd-order O_3 sensitivities to precursors in future works should elucidate and possibly isolate the sources, regions, reaction mechanisms and (if possible) the meteorological conditions that highly contribute or facilitate O_3-NO_x nonlinear relationship over YRD. This would greatly enhance the current and future O_3 pollution mitigation efforts in the YRD region and beyond.

Admittedly, this study still has some limitations. For example, the emissions inventory used in this study has uncertainties introduced by not considering sudden emissions. Moreover, the model performance of this study is affected by the uncertainty of the meteorological inputs generated by the WRF model, although we have validated our model against observed data. Regardless of the limitations, however, the insights and findings resulting from this study might be of interest to other city clusters in the world facing high ozone concentrations, as well as for evaluating mitigation strategies.

CRediT authorship contribution statement

Elly Arukulem Yaluk: Methodology, Software, Validation, Formal analysis, Investigation, Data curation, Writing – original draft, Visualization. **Yangjun Wang:** Conceptualization, Methodology, Software, Validation, Formal analysis, Investigation, Resources, Data curation, Writing – original draft, Writing – review & editing, Visualization, Supervision, Project administration, Funding acquisition. **Sen Jiang:** Data curation. **Ling Huang:** Software, Data curation. **Guibin Lu:** Investigation. **Ansheng Zhu:** Software. **Jinting Bian:** Data curation, Visualization. **Jin Xue:** Data curation, Visualization. **Yufei Du:** Visualization. **Nan Chen:** Visualization. **Kasemsan Manomaiphiboon:** Formal analysis, Visualization. **Hui Chen:** Writing – review & editing. **Kun Zhang:** Writing – review & editing. **Li Li:** Conceptualization, Methodology, Resources, Writing – review & editing, Supervision, Project administration, Funding acquisition.

Declaration of competing interest

The authors declare that they have no conflict of interest.

Data availability

Data will be made available on request.

Acknowledgements

This study was financially supported by the National Natural Science Foundation of China (No. 42075144 and 42005112), Open Foundation of State Environmental Protection Key Laboratory of Sources and Control of Air Pollution Complex (No. SCAPC202003) and the Shanghai International Science and Technology Cooperation Fund (No. 19230742500). We also appreciate the High-Performance Computing Center of Shanghai University and Shanghai Engineering Research Center of Intelligent Computing System (No. 19DZ2252600) for providing the computing resources and technical support.

Appendix A. Supplementary data

Supplementary data to this article can be found online at https://doi.org/10.1016/j.atmosenv.2023.119931.

References

An, J., Huang, Y., Huang, C., Wang, X., Yan, R., Wang, Q., Wang, H., Jing, S., Zhang, Y., Liu, Y., Chen, Y., Xu, C., Qiao, L., Zhou, M., Zhu, S., Hu, Q., Lu, J., Chen, C., 2021. Emission inventory of air pollutants and chemical speciation for specific anthropogenic sources based on local measurements in the Yangtze River Delta region, China. Atmos. Chem. Phys. 21, 2003–2025.

Arter, C.A., Arunachalam, S., 2021. Assessing the importance of nonlinearity for aircraft emissions' impact on O3 and PM2.5. Sci. Total Environ. 777, 146121.

Atkinson, R., 2000. Atmospheric chemistry of VOCs and NOx. Atmos. Environ. 34, 2063–2101.

Byun, D., Schere, K.L., 2006. Review of the governing equations, computational algorithms, and other components of the models-3 community Multiscale air quality (CMAQ) modeling system. Appl. Mech. Rev. 59, 51–77.

Cazorla, M., Herrera, E., Palomeque, E., Saud, N., 2021. What the COVID-19 lockdown revealed about photochemistry and ozone production in Quito, Ecuador. Atmos. Pollut. Res. 12, 124–133.

Clappier, A., Belis, C.A., Pernigotti, D., Thunis, P., 2017. Source apportionment and sensitivity analysis: two methodologies with two different purposes. Geosci. Model Dev. (GMD) 10, 4245–4256.

Cohan, D.S., Hakami, A., Hu, Y., Russell, A.G., 2005. Nonlinear response of ozone to emissions: source apportionment and sensitivity analysis. Environ. Sci. Technol. 39, 6739–6748.

Cohan, D.S., Napelenok, S.L., 2011. Air quality response modeling for decision support. Atmosphere 2, 407–425.

Collivignarelli, M.C., Abbà, A., Bertanza, G., Pedrazzani, R., Ricciardi, P., Carnevale Miino, M., 2020. Lockdown for CoViD-2019 in Milan: what are the effects on air quality? Sci. Total Environ. 732, 139280.

Fujita, E.M., Campbell, D.E., Stockwell, W.R., Saunders, E., Fitzgerald, R., Perea, R., 2016. Projected ozone trends and changes in the ozone-precursor relationship in the South Coast Air Basin in response to varying reductions of precursor emissions. J. Air Waste Manag. Assoc. 66, 201–214.

Gonçalves, M., Jiménez-Guerrero, P., Baldasano, J.M., 2009. Contribution of atmospheric processes affecting the dynamics of air pollution in South-Western Europe during a typical summertime photochemical episode. Atmos. Chem. Phys. 9, 849–864.

Guenther, A.B., Jiang, X., Heald, C.L., Sakulyanontvittaya, T., Duhl, T., Emmons, L.K., Wang, X., 2012. The Model of Emissions of Gases and Aerosols from Nature Version 2.1 (MEGAN2.1): an Extended and Updated Framework for Modeling Biogenic Emissions.

Hakami, A., Odman, M.T., Russell, A.G., 2003. High-order, direct sensitivity analysis of multidimensional air quality models. Environ. Sci. Technol. 37, 2442–2452.

Huang, X., Ding, A., Gao, J., Zheng, B., Zhou, D., Qi, X., Tang, R., Wang, J., Ren, C., Nie, W., Chi, X., Xu, Z., Chen, L., Li, Y., Che, F., Pang, N., Wang, H., Tong, D., Qin, W., Cheng, W., Liu, W., Fu, Q., Liu, B., Chai, F., Davis, S.J., Zhang, Q., He, K., 2020. Enhanced secondary pollution offset reduction of primary emissions during COVID-19 lockdown in China. Natl. Sci. Rev. 8.

Huang, Z., Hu, Y., Zheng, J., Yuan, Z., Russell, A.G., Ou, J., Zhong, Z., 2017. A new combined stepwise-based high-order decoupled direct and reduced-form method to improve uncertainty analysis in PM2.5 simulations. Environ. Sci. Technol. 51, 3852–3859.

Itahashi, S., Hayami, H., Uno, I., 2015. Comprehensive study of emission source contributions for tropospheric ozone formation over East Asia. J. Geophys. Res. Atmos. 120, 331–358.

Li, L., Chen, C.H., Huang, C., Huang, H.Y., Zhang, G.F., Wang, Y.J., Wang, H.L., Lou, S.R., Qiao, L.P., Zhou, M., Chen, M.H., Chen, Y.R., Streets, D.G., Fu, J.S., Jang, C.J., 2012. Process analysis of regional ozone formation over the Yangtze River Delta, China using the community multi-scale air quality modeling system. Atmos. Chem. Phys. 12, 10971.

Li, L., Li, Q., Huang, L., Wang, Q., Zhu, A., Xu, J., Liu, Z., Li, H., Shi, L., Li, R., Azari, M., Wang, Y., Zhang, X., Liu, Z., Zhu, Y., Zhang, K., Xue, S., Ooi, M.C.G., Zhang, D., Chan, A., 2020. Air quality changes during the COVID-19 lockdown over the Yangtze River Delta Region: an insight into the impact of human activity pattern changes on air pollution variation. Sci. Total Environ. 732, 139282.

Li, Q., Zhang, L., Wang, T., Wang, Z., Fu, X., Zhang, Q., 2018. "New" reactive nitrogen chemistry reshapes the relationship of ozone to its precursors. Environ. Sci. Technol. 52, 2810–2818.

Lian, X., Huang, J., Huang, R., Liu, C., Wang, L., Zhang, T., 2020. Impact of city lockdown on the air quality of COVID-19-hit of Wuhan city. Sci. Total Environ. 742, 140556.

Liu, T., Wang, X., Hu, J., Wang, Q., An, J., Gong, K., Sun, J., Li, L., Qin, M., Li, J., Tian, J., Huang, Y., Liao, H., Zhou, M., Hu, Q., Yan, R., Wang, H., Huang, C., 2020. Driving forces of changes in air quality during the COVID-19 lockdown period in the Yangtze River Delta region, China. Environ. Sci. Technol. Lett. 7, 779–786.

Liu, Y., Wang, T., Stavrakou, T., Elguindi, N., Doumbia, T., Granier, C., Bouarar, I., Gaubert, B., Brasseur, G.P., 2021. Diverse response of surface ozone to COVID-19 lockdown in China. Sci. Total Environ. 789, 147739.

Lu, X., Zhang, L., Wang, X., Gao, M., Li, K., Zhang, Y., Yue, X., Zhang, Y., 2020. Rapid increases in warm-season surface ozone and resulting health impact in China since 2013. Environ. Sci. Technol. Lett. 7, 240–247.

Miyazaki, K., Bowman, K., Sekiya, T., Jiang, Z., Chen, X., Eskes, H., Ru, M., Zhang, Y., Shindell, D., 2020. Air quality response in China linked to the 2019 novel coronavirus (COVID-19) lockdown. Geophys. Res. Lett. 47, e2020GL089252.

Muhammad, S., Long, X., Salman, M., 2020. COVID-19 pandemic and environmental pollution: a blessing in disguise? Sci. Total Environ. 728, 138820.

Ni, Z.Z., Luo, K., Gao, Y., Gao, X., Jiang, F., Huang, C., Fan, J.R., Fu, J.S., Chen, C.H., 2020. Spatial–temporal variations and process analysis of O3 pollution in Hangzhou during the G20 summit. Atmos. Chem. Phys. 20, 5963–5976.

Ordóñez, C., Garrido-Perez, J.M., García-Herrera, R., 2020. Early spring near-surface ozone in Europe during the COVID-19 shutdown: meteorological effects outweigh emission changes. Sci. Total Environ. 747, 141322.

Pei, Z., Han, G., Ma, X., Su, H., Gong, W., 2020. Response of major air pollutants to COVID-19 lockdowns in China. Sci. Total Environ. 743, 140879.

Sharma, S., Sharma, P., Khare, M., 2017. Photo-chemical transport modelling of tropospheric ozone: a review. Atmos. Environ. 159, 34–54.

Shehzad, K., Sarfraz, M., Shah, S.G.M., 2020. The impact of COVID-19 as a necessary evil on air pollution in India during the lockdown. Environ. Pollut. 266, 115080.

Shen, H., Sun, Z., Chen, Y., Russell, A.G., Hu, Y., Odman, M.T., Qian, Y., Archibald, A.T., Tao, S., 2021a. Novel method for ozone isopleth construction and diagnosis for the ozone control strategy of Chinese cities. Environ. Sci. Technol. 55, 15625–15636.

Shen, H., Sun, Z., Chen, Y., Russell, A.G., Hu, Y., Odman, M.T., Qian, Y., Archibald, A.T., Tao, S., 2021b. Novel method for ozone isopleth construction and diagnosis for the ozone control strategy of Chinese cities. Environ. Sci. Technol. 55, 15625–15636.

Shi, X., Brasseur, G.P., 2020. The response in air quality to the reduction of Chinese economic activities during the COVID-19 outbreak. Geophys. Res. Lett. 47, e2020GL088070.

Shu, L., Xie, M., Wang, T., Gao, D., Chen, P., Han, Y., Li, S., Zhuang, B., Li, M., 2016. Integrated studies of a regional ozone pollution synthetically affected by subtropical high and typhoon system in the Yangtze River Delta region, China. Atmos. Chem. Phys. 16, 15801–15819.

Sicard, P., De Marco, A., Agathokleous, E., Feng, Z., Xu, X., Paoletti, E., Rodriguez, J.J.D., Calatayud, V., 2020. Amplified ozone pollution in cities during the COVID-19 lockdown. Sci. Total Environ. 735, 139542.

Siciliano, B., Dantas, G., da Silva, C.M., Arbilla, G., 2020. Increased ozone levels during the COVID-19 lockdown: analysis for the city of Rio de Janeiro, Brazil. Sci. Total Environ. 737, 139765.

Sillman, S., He, D., 2002. Some theoretical results concerning O3-NOx-VOC chemistry and NOx-VOC indicators. J. Geophys. Res. Atmos. 107. ACH 26-21-ACH 26-15.

Sillman, S., West, J.J., 2009. Reactive nitrogen in Mexico City and its relation to ozone-precursor sensitivity: results from photochemical models. Atmos. Chem. Phys. 9, 3477–3489.

Skamarock, C., Klemp, B., Dudhia, J., Gill, O., Liu, Z., Berner, J., Wang, W., Powers, G., Duda, G., Barker, D.M., Huang, X., 2019. A Description of the Advanced Research WRF Model Version 4.

Tang, G., Liu, Y., Zhang, J., Liu, B., Li, Q., Sun, J., Wang, Y., Xuan, Y., Li, Y., Pan, J., Li, X., Wang, Y., 2021. Bypassing the NOx titration trap in ozone pollution control in Beijing. Atmos. Res. 249, 105333.

Tian, H., Liu, Y., Li, Y., Wu, C.-H., Chen, B., Kraemer, M.U.G., Li, B., Cai, J., Xu, B., Yang, Q., Wang, B., Yang, P., Cui, Y., Song, Y., Zheng, P., Wang, Q., Bjornstad, O.N., Yang, R., Grenfell, B.T., Pybus, O.G., Dye, C., 2020. An investigation of transmission control measures during the first 50 days of the COVID-19 epidemic in China. Science 368, 638–642.

Wang, H., Huang, C., Tao, W., Gao, Y., Wang, S., Jing, S., Wang, W., Yan, R., Wang, Q., An, J., Tian, J., Hu, Q., Lou, S., Pöschl, U., Cheng, Y., Su, H., 2022a. Seasonality and reduced nitric oxide titration dominated ozone increase during COVID-19 lockdown in eastern China. npj Climate and Atmospheric Science 5, 24.

Wang, L., Li, M., Yu, S., Chen, X., Li, Z., Zhang, Y., Jiang, L., Xia, Y., Li, J., Liu, W., Li, P., Lichtfouse, E., Rosenfeld, D., Seinfeld, J.H., 2020a. Unexpected rise of ozone in urban and rural areas, and sulfur dioxide in rural areas during the coronavirus city lockdown in Hangzhou, China: implications for air quality. Environ. Chem. Lett. 18, 1713–1723.

Wang, T., Xue, L., Brimblecombe, P., Lam, Y.F., Li, L., Zhang, L., 2017. Ozone pollution in China: a review of concentrations, meteorological influences, chemical precursors, and effects. Sci. Total Environ. 575, 1582–1596.

Wang, Y., Yaluk, E.A., Chen, H., Jiang, S., Huang, L., Zhu, A., Xiao, S., Xue, J., Lu, G., Bian, J., Kasemsan, M., Zhang, K., Liu, H., Tong, H., Ooi, M.C.G., Chan, A., Li, L., 2022b. The importance of NOx control for peak ozone mitigation based on a sensitivity study using CMAQ-HDDM-3D model during a typical episode over the Yangtze River Delta region, China. J. Geophys. Res. Atmos. 127, e2022JD036555.

Wang, Y., Yuan, Y., Wang, Q., Liu, C., Zhi, Q., Cao, J., 2020b. Changes in air quality related to the control of coronavirus in China: implications for traffic and industrial emissions. Sci. Total Environ. 731, 139133.

Wang, Y., Zhu, S., Ma, J., Shen, J., Wang, P., Wang, P., Zhang, H., 2021. Enhanced atmospheric oxidation capacity and associated ozone increases during COVID-19 lockdown in the Yangtze River Delta. Sci. Total Environ. 768, 144796.

Wang, Y.H., Hu, B., Ji, D.S., Liu, Z.R., Tang, G.Q., Xin, J.Y., Zhang, H.X., Song, T., Wang, L.L., Gao, W.K., Wang, X.K., Wang, Y.S., 2014. Ozone weekend effects in the Beijing–Tianjin–Hebei metropolitan area, China. Atmos. Chem. Phys. 14, 2419–2429.

Zhang, K., Liu, Z., Zhang, X., Li, Q., Jensen, A., Tan, W., Huang, L., Wang, Y., de Gouw, J., Li, L., 2022. Insights into the significant increase in ozone during COVID-19 in a typical urban city of China. Atmos. Chem. Phys. 22, 4853–4866.

Zhang, W., Capps, S.L., Hu, Y., Nenes, A., Napelenok, S.L., Russell, A.G., 2012. Development of the high-order decoupled direct method in three dimensions for

particulate matter: enabling advanced sensitivity analysis in air quality models. Geosci. Model Dev. (GMD) 5, 355–368.
Zhao, Y., Zhang, K., Xu, X., Shen, H., Zhu, X., Zhang, Y., Hu, Y., Shen, G., 2020. Substantial changes in nitrogen dioxide and ozone after excluding meteorological impacts during the COVID-19 outbreak in mainland China. Environ. Sci. Technol. Lett. 7, 402–408.
Zhu, S., Poetzscher, J., Shen, J., Wang, S., Wang, P., Zhang, H., 2021. Comprehensive insights into O3 changes during the COVID-19 from O3 formation regime and atmospheric oxidation capacity. Geophys. Res. Lett. 48, e2021GL093668.